

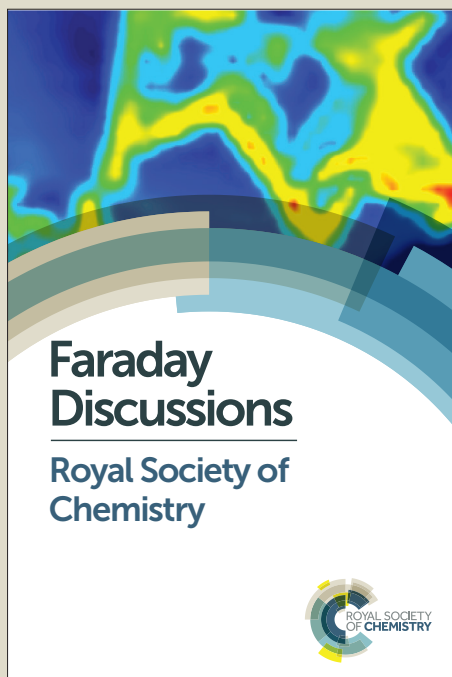
Faraday Discussions

Accepted Manuscript



This manuscript will be presented and discussed at a forthcoming Faraday Discussion meeting. All delegates can contribute to the discussion which will be included in the final volume.

Register now to attend! Full details of all upcoming meetings: <http://rsc.li/fd-upcoming-meetings>



This is an *Accepted Manuscript*, which has been through the Royal Society of Chemistry peer review process and has been accepted for publication.

Accepted Manuscripts are published online shortly after acceptance, before technical editing, formatting and proof reading. Using this free service, authors can make their results available to the community, in citable form, before we publish the edited article. We will replace this *Accepted Manuscript* with the edited and formatted *Advance Article* as soon as it is available.

You can find more information about *Accepted Manuscripts* in the [Information for Authors](#).

Please note that technical editing may introduce minor changes to the text and/or graphics, which may alter content. The journal's standard [Terms & Conditions](#) and the [Ethical guidelines](#) still apply. In no event shall the Royal Society of Chemistry be held responsible for any errors or omissions in this *Accepted Manuscript* or any consequences arising from the use of any information it contains.

Formation of New Polymorphs Without any Nucleation Step

Desolvation of the Rimonabant Monohydrate: Directional Crystallisation Concomitant to Smooth Dehydration

Baptiste Fours, Yohann Cartigny, Samuel Petit and Gérard Coquerel*

DOI: 10.1039/b000000x [DO NOT ALTER/DELETE THIS TEXT]

Rimonabant monohydrate can be dehydrated at 100°C or above with
10 complete loss of structural information; in this case the amorphous material
can lead to nucleation and crystal growth. The water molecules can also be
removed by a smooth process below T_g (78°C) of the anhydrous phase. In
that latter process there is a structural filiation between the mother phase
and the daughter phase. The solvent molecules escape from the mother
15 structure by using a network of specific channels; the new non solvated
material undergoes a relaxation process similar to a directional
crystallization. By this soft mode of desolvation inside a material which has
a very limited mobility, the nucleation of a non-solvated material can be
avoided. The structural information contained in the mother phase is not
20 used as a template for crystal growth but it is more a progressive
rearrangement of the new desolvated material towards the nearest well in
energy. Thus, a metastable new polymorph of a non-solvated component
can be obtained by: (i) the crystallization of the component as a solvate and
(ii) a smooth desolvation at $T < T_g$. Other parameters susceptible to interfere
25 with that transmission of structural information are discussed.

Introduction

Crystal polymorphism of molecular compounds is usually assumed to be determined
by the nucleation step,¹ as soundly deduced in the 90's from puzzling phenomena
such as 'disappearing polymorphs'² and 'concomitant polymorphs'.³ However the
30 fundamental mechanisms at a molecular level of nucleation from solution remain
insufficiently understood and constitute a subject of controversial discussions,⁴
mainly related to the difficulty of exploring the size range (and possibly time scale)
of nucleation with suitable experimental techniques.⁵

In order to get new insights into nucleation mechanisms, it is therefore of high
35 interest to consider situations in which spontaneous nucleation can be either
triggered or inhibited by imposing suitable environmental conditions. In that respect,
desolvation processes might constitute an interesting situation since their associated
mechanism(s) can involve (or not) a nucleation step after a more or less cooperative
departure of solvent molecules from the initial crystal packing.

Almost twenty years ago, a so-called ‘unified model for the dehydration of molecular crystals’ was proposed, in which four criteria were identified as decisive parameters for cooperative or destructive mechanisms.⁶ These views have been reinforced by other consistent classifications based on strictly structural⁷ or phenomenological approaches.⁸

In the present paper, it is suggested that a thorough analysis of desolvation behaviours as well as the use of suitable criteria may constitute valuable methodological tools for the study of systems in which crystallisation might occur either without nucleation (by means of a cooperative mechanism involving a structural filiation) or with nucleation (and growth) when operating conditions do not meet predefined criteria. This approach, here applied to a monohydrated form of the pharmaceutical ingredient Rimonabant (Figure 1) is a first step toward a putative better control of the nucleation step in the frame of solid-solid transformations, and might be used as a rational strategy for the design of new polymorphs.

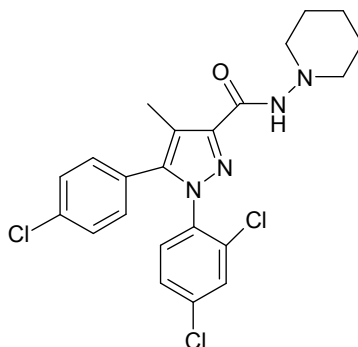


Figure 1. Developed formula of Rimonabant: N-piperido-5-(4-chlorophenyl)-1-(2,4-dichlorophenyl)-4-methylpyrazole-3-carboxamide.

Rimonabant was an API developed by Sanofi-Aventis for alcohol and drug withdrawal. After some years this active pharmaceutical ingredient has been itself withdrawn from market. Likewise many pharmaceutical substances, Rimonabant exhibits polymorphism. Two modifications (form I, $T_m=156.3$ °C and form II, $T_m=156.8$ °C) have been identified prior to this work.⁹ These two polymorphs are very close in energy whatever the temperature so that they appeared almost as isoenergetic varieties. After melting and quenching a glass is obtained with a T_g at 78°C (mid point transition – see ESI). Moreover, like other pharmaceuticals (*e.g.* olanzapine¹⁰), Rimonabant shows a great ability to form solvates. The list below gives an idea of these solvent molecules able to become a partner of crystallisation: water; methanol, ethanol, 2-methoxyethanol, isopropanol, 1-methyl butanol, DMF, NMP, DMSO, methylcyclohexane (2 polymorphs), dimethylacetamide, 1,4 dioxane. This is by no mean an exhaustive list and only ketones have resisted to give any solvate. This study is focused on the monohydrate only.¹¹

Experimental section

Crystalline samples of Rimonabant were provided by the Sanofi-Aventis Company, with a chemical purity higher than 99%. The monohydrated form was produced by

dissolving 8 g of Rimonabant in 40 g of acetone at room temperature. Then, 10 g of water were added dropwise and the monohydrate crystallized out spontaneously. Temperature can be dropped to 5°C to improve the yield (6.5 g after filtration) and drying to a fixed composition in water 3.7% w/w. Single crystals with a needle-like shape were obtained by slow evaporation at RT of the same acetone/water solution.

X-ray Powder Diffraction (XRPD)

XRPD analyses were performed using a D8 diffractometer (Bruker, Germany) equipped with a modified goniometer of reverse-geometry (- θ / θ)¹² and a LynxEye® detector (Bruker, Germany). Using Cu K α ($\lambda=1.54059$ Å) with a tube voltage and amperage set at 40 kV and 40 mA respectively, XRPD analyses were performed with a step of 0.04°(2 θ), and a 4 s/step counting time from 3 to 30° (2 θ).

Single Crystal X-ray Diffraction (SC-XRD)

The selected single crystal was stuck on a glass fibre and mounted on the full three-circle goniometer of a Bruker SMART APEX diffractometer equipped with a CCD area detector and operating with Mo K α_1 ($\lambda=0.71071$ Å) as incident beam. The SMART software¹³ was used to determine the cell parameters and the orientation matrix. Intensities were integrated and corrected for Lorentz polarization and absorption effects using SAINT software.¹³ The structure was solved by direct methods using the SHELX-97 suite of program,¹⁴ and anisotropic displacement parameters were refined for all non-hydrogen atoms. All hydrogen atoms were located by Fourier-difference synthesis and fixed geometrically according to their environment with a predefined isotropic thermal factor

Thermal Analysis (TGA and DSC)

Thermogravimetric-Differential Scanning Calorimetry (TG-DSC) measurements were carried out by using a Netzsch STA 449C Jupiter apparatus (Selb, Germany). The purge gas was helium (flow = 40 mL.min⁻¹) and the reference material was an empty covered aluminium pan. Enthalpy and temperature calibrations were performed with biphenyl and indium. The samples (5 mg \pm 0.05 mg) were weighed in covered pierced aluminium pans, and then placed in the analyser. Analyses were performed in the temperature range 20°C-150°C using a 5 K.min⁻¹ heating rate. After acquisition, the PROTEUS software was used for data processing (v. 4.8.4)

Dynamic Vapour Sorption (DVS)

Moisture sorption isotherms at 20°C of the monohydrate and the amorphous form were obtained by using a DVS-1 automated water sorption analyser (Surface Measurement Systems, Alpertown, U.K.). About 2 mg of solid were placed in the analyser for each experiment. Mass variations were recorded while relative humidity (R.H.) was successively decreased or increased from 90% to 0% R.H. by adapted steps of R.H. The automated analyser was allowed to proceed with the following step as soon as the mass variation of the sample was less than 5 10^{-4} %.min⁻¹.

Optical Microscopy Analysis of Single Crystals

Crystal morphology was observed by optical microscopy using a Hirox high resolution numerical microscope which enables a magnification up to $\times 7000$. The evolution of the observed crystals as a function of temperature was monitored with a

CCD camera coupled to the microscope and connected to a computer. The cooling or heating rates 5 K/min were controlled with a THMS 600 hot-stage setup (Linkham).

Results and Discussion

After preparation of the monohydrated form of Rimonabant from an acetone/water solution, single crystals of sufficient quality and size could be obtained and the crystal structure was analysed at room temperature (table 1, structure deposited in the CSD as CCDC 1033743). It could be established by X-ray diffraction that the main axis of the elongated single crystals corresponds to the crystallographic *a* axis. The asymmetric unit in the structure contains two molecules with different conformations, as illustrated in figure 2. They mainly differ by the orientation of the 4-chlorophenyl and 2,4-dichlorophenyl substituents with reference to the pyrazole ring. Figure 3 depicts the packing of the monohydrate, with two independent water molecules connected to the independent Rimonabant molecules (labelled A and B) via their amide groups. When considering only the H-bonds as intermolecular interactions, this pattern, as schematized in figure 4, induces the existence of Periodic Bond Chains (PBCs) running along the *b* axis, which is in apparent contradiction with the main direction of crystal development. One can see from Figure 3 that this stoichiometric hydrate constitutes a channel hydrate owing to the definition of Morris.⁷

Table 1. Crystal data and refinement parameters for Rimonabant monohydrate.

Formula	C ₂₂ H ₂₁ Cl ₃ N ₄ O.H ₂ O
Molecular weight (g.mol ⁻¹)	481.79
CCDC deposition number ^a	CCDC 1033743
T (K)	296
Wavelength (Å)	0.71073
Crystal dimension (mm)	2 × 0.2 × 0.2
Crystal morphology	Colourless needle
System	Triclinic
Space group	<i>P</i> -1
<i>a</i> (Å) α (°)	7.4245(5) 96.898(1)
<i>b</i> (Å) β (°)	13.2237(8) 96.177(1)
<i>c</i> (Å) γ (°)	24.718(2) 90.664(1)
Z, Z'	4, 2
V (Å ³)	2394.5(3)
d _{calc} (g.cm ⁻³)	1.336
μ (mm ⁻¹)	0.408
F ₀₀₀	1000
θ range (°)	1.55 to 26.43
h, k, l ranges	-9/9, -16/15, -30/30
Nb of collected / unique reflections	19375 / 9674
Nb of reflections (I>2σI) / parameters	4953/ 585
Residual electronic density (e.Å ⁻³)	+0.233 / -0.225
R ₁ , wR ₂ (I>2σI) ^b	0.0453, 0.0950
R ₁ , wR ₂ (all data)	0.0928, 0.1072

Goodness of fit 0.829

Table 2. Geometric parameters of hydrogen bonds in the structure of Rimonabant monohydrate (see atom labelling in Figure 2).

Hydrogen bond	(D \cdots A) (Å)	(D-H \cdots A) (°)	(H \cdots A) (Å)
N _{1A} -H _{1A} \cdots O _{wA}	2.89	177.4	2.05
N _{1B} -H _{1B} \cdots O _{wB}	2.86	172.7	2.02
O _{wA} -H _{wA} \cdots O _{1B}	2.76	167.4	2.01
O _{wB} -H _{wB} \cdots O _{1A}	2.65	169.3	1.82
O _{wB} -H _{wB} \cdots N _{2B}	2.95	/	/
O _{wA} -H _{2A} \cdots N _{2A}	3.11	/	/

5

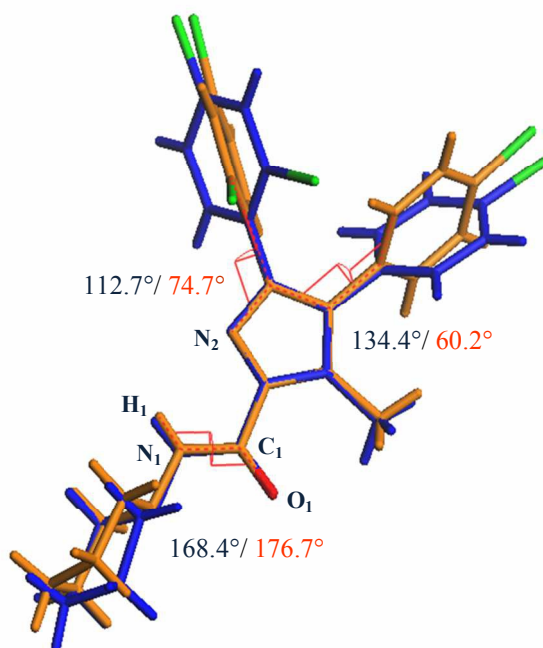


Figure 2. Comparison between the conformations of the two independent molecules in the crystal structure of Rimonabant monohydrate.

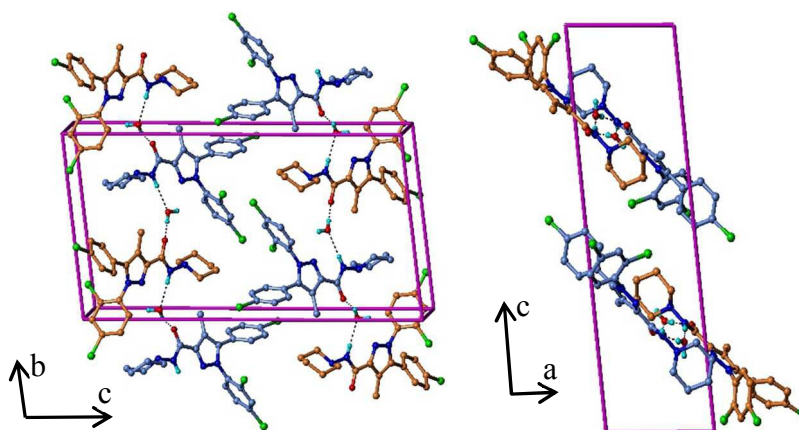


Figure 3. Crystal packing and H-bond network involving the two independent molecules (A: orange; B: blue) in the monohydrated structure of Rimobant.

5

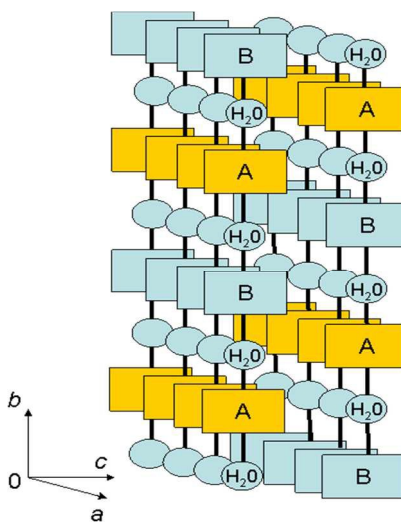


Figure 4. Schematic representation of Rimobant monohydrate as a stoichiometric channel hydrate.

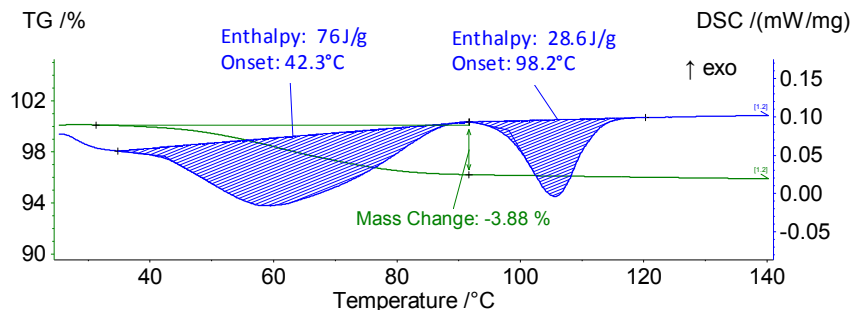
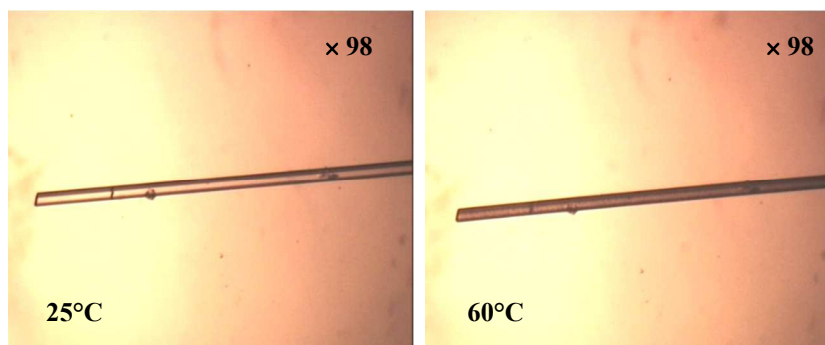


Figure 5. TGA (green curve) DSC (blue curve) of Rimonabant monohydrate (heating rate 5K/min under a constant flow of helium).

5 The thermal behavior of the monohydrate is displayed in figure 5. The dehydration starts at *ca.* 40°C, and the mass loss is completed by 90°C when heating is operated at 5K/min. The mass loss fits well with the expected value for a monohydrate *i.e.* 3.77% w/w. Close to the end of the dehydration, another large endothermic phenomenon takes place. TR-XRPD with similar experimental
 10 conditions shows above *circa* 100°C a flat XRPD pattern leading to the hypothesis that the second phenomenon is actually the melting of the new anhydrous material. Softer desolvation conditions were also tested such as: exposure to P₂O₅ in a close chamber at room temperature (RT), constant flow of dry nitrogen at RT, isotherm at 60°C. (*i.e.*, 18°C below Tg). Figure 6 displays at various magnifications the initial
 15 state and the final state of the dehydration under soft conditions: isotherm at 60°C under normal pressure. The initial single crystal is transparent; it shows the morphology of the particle which is elongated along *a* axis. After a while the crystal becomes translucent. At greater magnifications (× 320 and then × 2100) it appears that the initial needle has been segmented, more or less periodically, into small
 20 regions of some micrometers long. The channels containing the water molecules being parallel to the main axis of the needle, it is not surprising with this set of kinetic parameters that water molecules could find a short cut.



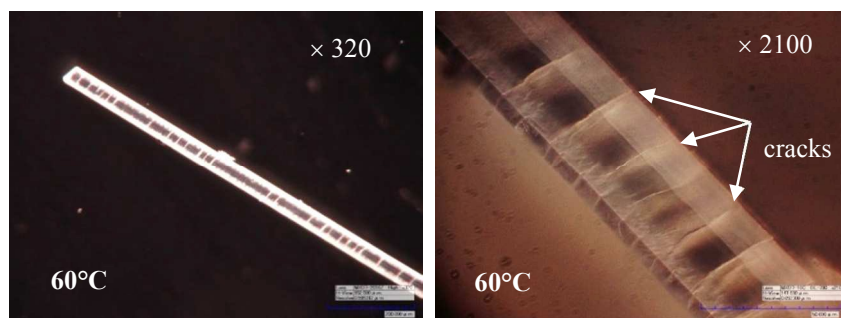
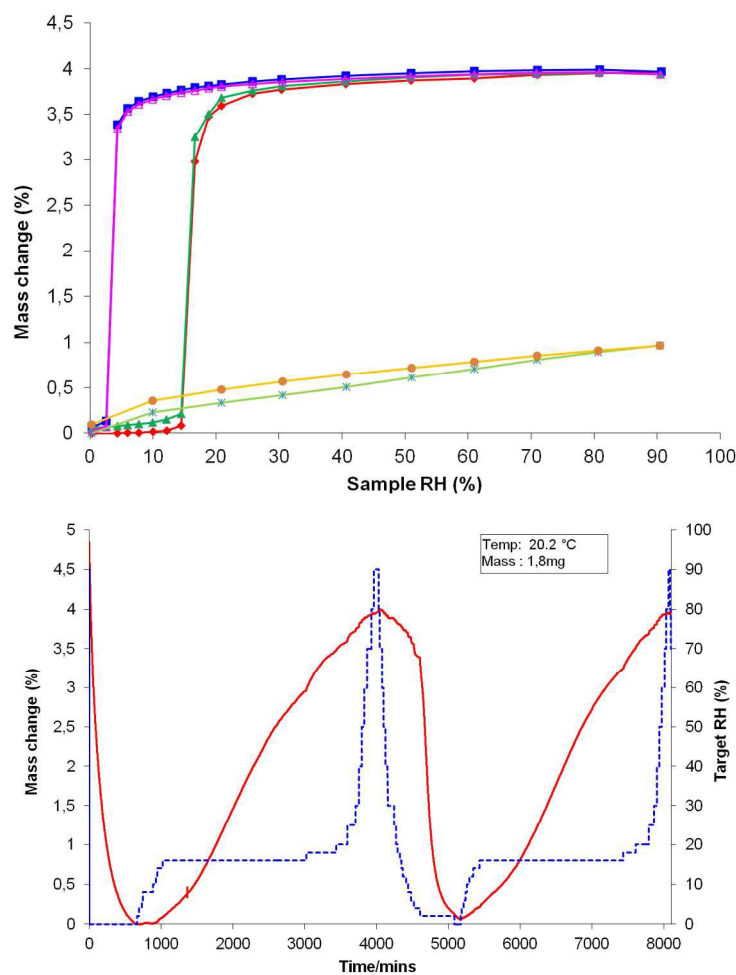


Figure 6. Optical microscopy photographs showing a single crystal of Rimonabant monohydrate undergoing dehydration in smooth conditions (upper part). The macroscopic consequences of dehydration at 60°C are shown at higher magnification (lower part).

Figure 7 shows several cycles of sorption and desorption of moisture at 20°C (DVS studies) from 0% to 90% Relative Humidity (RH). Starting from the monohydrate at 90% RH, it shows that this phase is stable at 20°C down to 4% RH. On sorption, a sharp take-off appears at 14% RH demonstrating the reversibility of the dehydration and rehydration when operated under smooth conditions. Even though the mass versus RH graph shows two abrupt events with hysteresis, the time-resolved corresponding representation shows that actually, for a small mass (1.8mg), the desorption and sorption of water molecules required several thousands of minutes for completion when operated smoothly under a constant flow of nitrogen with a precise RH. By contrast, if these cycles are performed on the amorphous API obtained after a dehydration up to 100°C and cooling down to RT, no stepped evolution is obtained even after more than 2×2000 minutes per cycle. In a more general way, we never observed the spontaneous nucleation of the monohydrate by sorption of humidity on the following starting materials: amorphous state, form I and form II, even after inoculation of the monohydrate at 20°C (see ESI for DVS analyses of forms I and II). Rimonabant shows a poor hydrophilicity; there is thus a weak plasticizing effect and this can, at least partly, explain the difficulty of crystallizing the monohydrate by means of amorphous – vapor interactions.



5 Figure 7. DVS studies at 20°C of Rimonabant showing the monohydrate-anhydrous equilibria (blue; pink, dark green and red isotherms). In the upper part, the green and orange curves illustrate the absence of evolution (limited to a weak adsorption) for the amorphous form under the same conditions. The lower part shows the time-resolved DVS evolution for successive dehydrations and rehydrations (red: mass
10 variations, dashed blue line: RH variations).

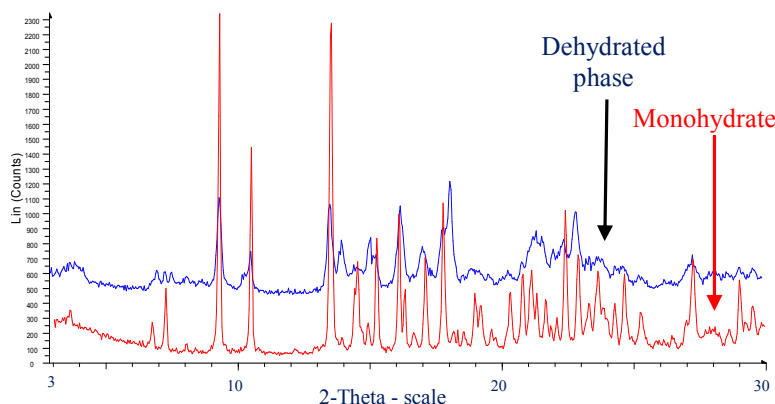
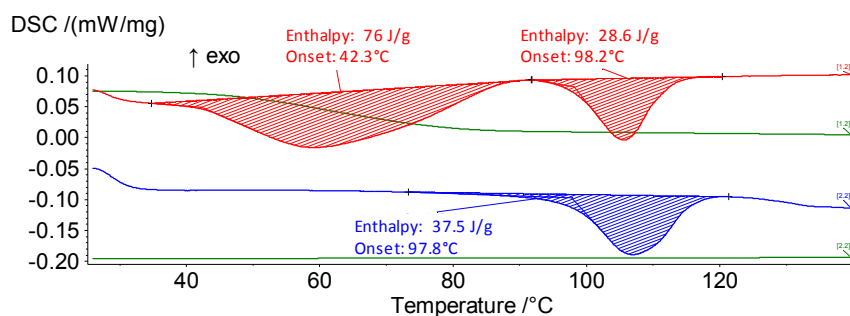


Figure 8. XRPD patterns of the monohydrate and smoothly dehydrated forms of Rimobant.

5 Figure 8 shows the XRPD patterns of the monohydrate and the anhydrous phase obtained by desolvation at room temperature via desorption of water in a close vial with P_2O_5 . Even if the crystallinity of the dehydrated phase has dropped, the filiation of structural information is rather obvious. Thus, it can be concluded that smooth desolvation of this channel hydrate below T_g leads to a crystallized phase with a clear structural filiation with the mother phase, and the situation looks like a case of
 10 'isomorphic desolvate' similar to those studied by Stephenson *et al.*¹⁵ Figure 9 shows the superimposition of the monohydrate behavior and that of the anhydrous phase resulting from the soft dehydration below T_g . The TGA profile of the anhydrous form is indeed flat and the endothermic phenomenon at $98 \pm 0.2^\circ\text{C}$ (onset
 15 temperature) is the metastable fusion of what has to be defined as a new polymorph H (to recall that it comes from the desolvation of the monohydrate). The melting temperature of form H is thus 60°C below that of forms I (156.3°C) and II (156.8°C).



20 Figure 9. Comparison of the TGA and DSC curves for the monohydrated (upper)

and smoothly dehydrated (lower) forms of Rimonabant (heating rate 5 K/min).

From this experimental study we can conclude that the dehydration of the Rimonabant monohydrate depends on the environmental conditions applied. If the dehydration is performed above 100°C a complete destruction of the initial phase occurs and the system will suffer from a complete amnesia about the former structural order. A reappearance of structural order will need to proceed through a nucleation and growth process. By contrast, if a smooth dehydration is performed below T_g (78°C) there is a transmission of structural information between the mother phase (monohydrate crystal lattice) and the new metastable polymorph H so no nucleation is needed. A schematic representation of such behaviour is proposed in Figure 10, and illustrates the possibility to identify new polymorphic forms, as recently shown in the case of Paroxetine HCl.¹⁶

Concerning Rimonabant, the channel hydrate has probably some degrees of elasticity to ensure the release of water molecules. Nevertheless, these channels are aligned along the long axis of the needle making the pathways for a release in the gas phase a too long voyage. The defects perpendicular to a axis can be used as short cuts. It is remarkable that under the environmental conditions used for the desolvation, the needle is segmented by periodic cracks and in between these large defects there are others small cracks more or less periodic as well. It is likely that the free migration path in the crystal lattice depends on the driving force for desolvation.

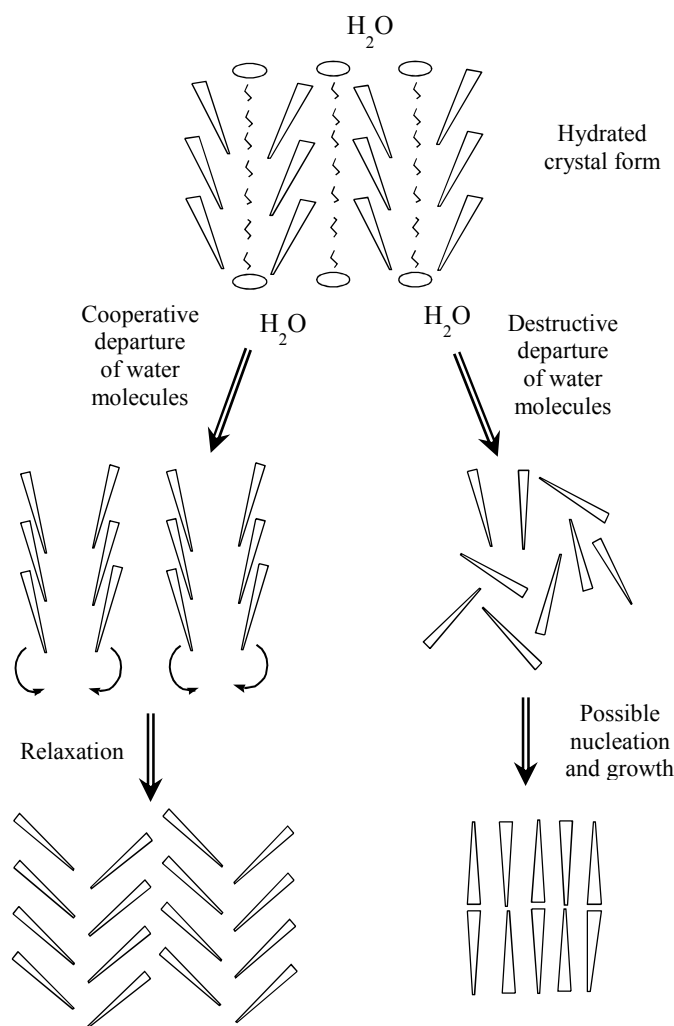
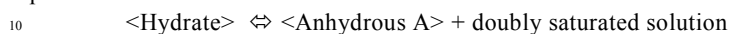


Figure 10. Schematic representation showing the possibility to produce different crystal forms and possibly amorphous material by means of distinct dehydration mechanisms from a channel hydrate.

5

Extended Discussion

Many hydrates lead to a schematic binary system displayed in figure 11a with a so-called non congruent fusion. The hydrate is stable up to T_p , the temperature of the peritectic transition:¹⁷



Even if it sounds weird, it is then perfectly possible to desolvate a hydrate in aqueous solution if the temperature of the system is adjusted above T_p .

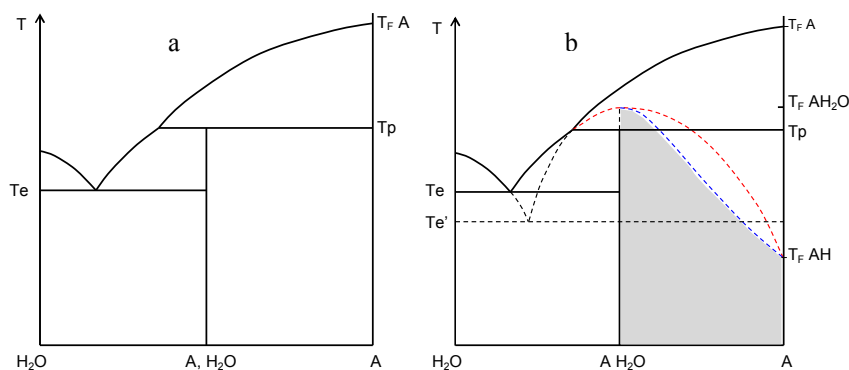


Figure 11. (a) stable equilibria involving a stoichiometric monohydrate with its reversible decomposition at the peritectic temperature T_p (non-congruent fusion). Figure 11b represents, in addition to the stable equilibria, the metastable equilibria including: the congruent fusion at $T_F A H_2 O$, the grey zone represents the domain of the non-stoichiometric phase spanning from pure A –up to $T_F A H$ – to $A H_2 O$. This monophasic domain could be labelled $\langle A(H_2O)_x \rangle$ with $0 \leq x \leq 1$.

The schematic binary system displayed in figure 11b represents the corresponding metastable congruent fusion at $T_F A H_2 O$ and starting from that point a metastable liquidus (in red dashed line) and solidus (in blue dashed line) converge to the metastable melting point of A_H at $T_F A_H$. Dehydration or re-hydration corresponds to the crossing of the monophasic domain $\langle A(H_2O)_x \rangle$ with $0 \leq x \leq 1$ i.e. a non-stoichiometric hydrate (*i.e.* continuum in composition) whose crystal lattice features versus x show little changes if any. This situation should be distinguished from a physical mixture of hydrated and anhydrous forms, that may also exist as intergrown domains. In the case of a dynamic solid solution envisaged here, the access to the putative polymorph A_H implies other requirements to be fulfilled. The glass transition is correlated with molecular mobility and thus a safe way to access to A_H is to complete the desolvation below T_g so that the new anhydrous material is ‘frozen’ with some limited abilities to re-arrange from the purely isomorphous desolvate to the local bottom in energy. It should however be highlighted that water activity may decrease the temperature of glass transition through a plasticizing effect, so the residence time of water in the sample may affect the dehydration behaviour in smooth conditions.¹⁸

The access to A_H is thus conditioned by a set of 4 temperatures: Temperature of fusion of the stable form (no other metastable form than A_H is considered for clarity), the temperature of fusion of the metastable form A_H , the temperature of the glass transition T_g and the temperature of desolvation. Some combinations only are discussed below:

$$T_F A > T_F A_H > T_g > T_{\text{desolvation}}$$

This case has been treated in this experimental study. If the crystals are not excessively large and thus the residence time of the solvent molecules out of their crystallographic sites is short,¹⁸ there is a good probability that a new desolvated phase appears. This anhydrous form can be obtained only by a smooth release of the

volatile partner of crystallization. Therefore, an exhaustive exploration of the landscape of a molecule (survey of its unary system) needs to go through investigations of several binary systems with volatile solvents in view to crystallize solvates. Smooth desolvations at a temperature below T_g and the temperature of fusion of this desolvated phases lead to new crystal packings impossible to obtained by simple adjustments of T and P in the unary system.

$$T_{FA} > T_{\text{desolvation}} > T_{FA_H} > T_g$$

This is also a case exemplified in this study. Because of the ‘high’ temperature of desolvation, the dehydrated material has lost the structural information contained in the solvated phase. The material is ready for nucleation and crystal growth of the stable anhydrous form.¹⁹

$$T_{FA} > T_g > T_{FA_H} > T_{\text{desolvation}}$$

In that interesting case the temperature of fusion of the desolvated phase is clearly below the T_g of the anhydrous phase. If the release of solvent molecules is smooth and fast enough, the resulting phase will still contain long range order. But in that particular case the amorphous solid is more stable than this flimsy crystallized phase. On ageing the crystallized phase will collapse progressively. This phenomenon called superheating has been observed with alpha trehalose.²⁰ It is even possible to speed up the desolvation at a temperature above T_{FA_H} but still below T_g for a limited period of time (*i.e.* $T_{FA} > T_g > T_{\text{desolvation}} > T_{FA_H}$) and to observe this superheated crystallized phase.

Conclusion

The experimental part of this communication gives evidence that Rimonabant monohydrate can be desolvated with a complete loss of structural information of the former crystallized phase (*e.g.* by heating up to 100°C). The subsequent evolution must go through a nucleation and crystal growth process.

The monohydrate can also be submitted to a smooth desolvation process below T_g of the anhydrous phase which leads to a new polymorph A_H exhibiting a clear structural filiation with the mother hydrated phase. The relaxation of the solid after departure of the water molecules is ensured by directional cooperative movements; there is no need for nucleation and growth of this metastable phase whose melting point is 60°C below that of the two, almost iso-energetic, polymorphs I and II.

Extension of these data to desolvation mechanism is proposed by considering the following 4 temperatures: temperature of fusion of the stable form T_{FA} , the temperature of fusion of the metastable form A_H , the temperature of the glass transition T_g and the temperature of desolvation. A prediction of the outcome of a desolvation is possible by considering the order of T_{FA} , T_g , T_{FA_H} and $T_{\text{desolvation}}$.

Of course other parameters such as: crystallinity of the initial phase, crystal structure, crystal size distribution of the solvate, mode of desolvation, etc. have an impact on the course of the desolvation but the order of these 4 temperatures gives a guide to predict the likelihood of the desolvation mechanism.

One of the general consequences of this scheme is that a thorough investigation of the solid phases of a pure component (unary system) should include the search for

solvates with volatile solvents. If some of them exist they could be desolvated at a temperature below T_g and $T_{FA_desolvate}$ (e.g. $T_{FA} > T_{FA_desolvate} > T_g > T_{desolvation}$) to produce metastable phases when compared to other polymorphs obtained from a solution or from the molten state. Their crystallographic features have some
 5 filiations with the corresponding solvates. These phases are not accessible directly in the unary system. Therefore, the experimenter needs to explore binary systems before going back to the pure component with the original packing(s).

Acknowledgements

Sanofi is thanked for its support to this study.

10 References

- Normandie Université; EA 3233 SMS, Crystal Genesis Unit, University of Rouen, F-76821 Mont Saint Aignan, France. Fax-Tel: 33 23552 2927; E-mail: gerard.coquerel@univ-rouen.fr
- † Electronic Supplementary Information (ESI) available: [CIF file for the crystal structure of Rimonabant monohydrate; DSC curve showing the glass transition for the amorphous form of
 15 Rimonabant; DVS results of Rimonabant forms I and II at 20 °C]. See DOI: 10.1039/b000000x/
- 1 J. Bernstein, *Polymorphism in Molecular Crystals*, IUCr Monographs on Crystallography 14; Clarendon Press: Oxford, 2002; T. L. Threlfall, *Analyst*, 1995, **120**, 2435.
 - 2 J. D. Dunitz and J. Bernstein, *Acc. Chem. Res.*, 1995, **28**, 193.
 - 20 3 J. Bernstein, R. J. Davey and J.-O. Henck, *Angew. Chem. Int. Ed.*, 1999, **38**, 3440.
 - 4 A. Gavezzotti, *Chem. Eur. J.*, 1999, **5**, 567; D. Erdemir, A. Y. Lee and A. S. Myerson, *Acc. Chem. Res.*, 2009, **42**, 621; R. J. Davey, S. L. M. Schroeder and J. H. ter Horst, *Angew. Chem. Int. Ed.*, 2013, **52**, 2.
 - 5 P. G. Vekilov, *Cryst. Growth Des.*, 2004, **4**, 671.
 - 25 6 S. Petit and G. Coquerel, *Chem. Mater.*, 1996, **8**, 2247.
 - 7 K. R. Morris, *Structural aspects of hydrates and solvates*. in: Brittain, H.G. (Ed.), *Polymorphism in Pharmaceutical Solids*, 95. Marcel Dekker: New York, 1999, 125.
 - 8 A. K. Galwey, *Thermochim. Acta*, 2000, **355**, 181.
 - 9 B. J. Venhuis, M. V. Vredenburg, N. Kaun, J. K. Maurin, Z. Fijałek and D. de Kaste, *J. Pharm. Biomed. Anal.*, 2011, **54**, 21.
 - 30 10 C. Cavallari, B. Pérez-Artacho Santos and A. Fini, *J. Pharm. Sci.*, 2013, **102**, 4046.
 - 11 G. Coquerel, H. Duplaa, B. Fours, O. Monnier and P. Ochsenein, *Monohydrate of rimonabant, preparation method thereof and pharmaceutical compositions containing same*, Patent WO 2007/090949.
 - 35 12 G. Coquerel, M. Sanselme and A. Lafontaine, *Method and measuring scattering of X-rays, its applications and implementation device*. Patent WO2012/136921 A1, 2012.
 - 13 Bruker AXS Inc., Bruker SMART (5.059) and SAINT (6.01), 1997, *Madison, Wisconsin*
 - 14 G. M. Sheldrick, SHELXS97 and SHELXL97, *Institut für Anorganische Chemie der Universität: Göttingen, Germany*, 1997.
 - 40 15 G. A. Stephenson, E. G. Groleau, R. L. Kleemann, W. Xu, and D. R. Rigsbee, *J. Pharm. Sci.* 1998, **87**, 536.
 - 16 M. F. Pina, M. Zhao, J. F. Pinto, J. J. Sousa, C. S. Frampton, V. r Diaz, O. Suleiman, L. Fábian, and D. Q. M. Craig, *Cryst. Growth Des.*, 2014, **14**, 3774.
 - 17 G. Coquerel, *Chem. Soc. Rev.*, 2014, **43**, 2286.
 - 45 18 Y. Amharar, S. Petit, M. Sanselme, Y. Cartigny, M.-N. Petit and G. Coquerel, *Cryst. Growth Des.*, 2011, **11**, 2453.
 - 19 M. Descamps and E. Dudognon, *J. Pharm. Sci.*, 2014, **103**, 2615.
 - 20 J. F. Willart, A. Hedoux, Y. Guinet, F. Danede, L. Paccou, F. Capet and M. Descamps, *J. Phys. Chem. B*, **2006**, *110*, 11040.

50